Supplementary Materials

Of

Electromagnetic Brain Source Imaging by Means of a Robust Minimum Variance Beamformer

Seyed Amir Hossein Hosseini, Abbas Sohrabpour, *Student Member*, *IEEE*, Mehmet Akçakaya, *Member, IEEE,* and Bin He*, *Fellow, IEEE*

A. Convex Optimization

Convex optimization solvers, including CVX, employ a multitude of algorithms to solve optimization problems formulated as being convex. Interior point methods are famous algorithms used to solve convex optimization problems in general and second-order cone programs (SOCP) in particular [1]. These methods define a so-called "barrier function" that basically transforms constrained optimization problems into unconstrained ones. These methods impose a condition on the goal function of the transformed unconstrained optimization problem, that it cannot result in solutions that do not satisfy the constraints of the original optimization problem by penalizing solutions that get close to the constraint boundary (in limit penalizing solutions on the constraint boundary by infinity), hence creating a barrier that does not let the solution to pass which ensures the satisfaction of the constraint. How SOCP problems are tackled can be found in great details in [2]. The details of these algorithms have been well studied and practiced in the literature and given the limited space we have in the paper and our primary focus on the source imaging applications in this paper, and the wide use of these techniques and solvers in the optimization field, we refer the interested reader to the optimization literature for further reading and investigation [1], [2].

B. Time-courses of Activity

Refer to Fig. S1 and Fig. S2.

C. Practical Considerations

In this section, some considerations regarding the implementation of the beamformers in general and its robust version in particular will be discussed. The accuracy of the covariance estimation plays a crucial role in the ultimate performance of the beamformers. On the other hand, the empirical estimation can poorly represent the true covariance matrix, if the number of data points is not sufficiently large. To address this issue, many techniques have been developed to regularize and purify the estimation [3]. In this study, a technique based on shrinkage models [3] was used to estimate the covariance matrices of the measurements, noise and uncertainty regions.

Another issue that requires attention is the size of the uncertainty region for each voxel with respect to the size of the lead field column. The uncertainty ellipsoid should not be too large to include the origin; otherwise, the constraint in (8) becomes infeasible, which in turn makes the problem unsolvable. On the other hand, a non-conservative inflation of the uncertainty ellipsoid can degrade the performance. This issue is pronounced even more in a fixed orientation model as is the case of this study, since in such a model orientations may vary drastically within each region depending on the size and location of the uncertainty region. Therefore, a constricting mechanism is required to ensure that each uncertainty ellipsoid does not grow larger than necessary. To this end, we defined the parameter β_i for each voxel as the ellipsoid radius along the direction $k_i/\|k_i\|$ normalized by $\|k_i\|$. This

parameter, which measures the size of the ellipsoid with respect to the distance of its center from the origin, can be calculated as:

$$\beta_i = \frac{1}{\sqrt{k_i^T P_i^{-1} k_i}}, \quad \forall\, i \in \{1, \dots, N\}. \tag{1}$$

Each uncertainty ellipsoid can then be rescaled such that its β_i-parameter is no larger than a cut-off value. The threshold can be determined either upfront or in an automated manner such as the mean of all β_i-parameters that are less than 1 (of the ellipsoids that do not contain the origin). In this study, the latter approach was used. Fig. S3 (A), which plots the histogram of the β_i-parameters, provides information regarding the distribution of the mentioned parameter for all voxels as well as the position of the cut-off value in this distribution. In Fig. S3 (B), the parameter β_i of all voxels versus the standard deviation (STDev) of the angles within the uncertainty region (not corrected by β_i) is plotted. This plot shows that the higher the variance in the orientation of the dipoles within the uncertainty region (due to the convoluted cortex), the larger its size will be. When there is a higher degree of variance among the lead field vectors in the neighborhood of a point, the uncertainty region has to be large enough to encompass all such points; which inadvertently results in a higher parameter β_i. Thus to relieve the situation different remedies can be applied; one is to look at smaller neighborhoods around any given point to calculate the covariance. This will result in less variance but the sample size will also decrease, and consequently the estimation will be less accurate. Another approach is to use a rotational model and not fix the dipole orientation, which makes the problem size larger by a factor of three and can deviate from biophysical models regarding the generation of M/EEG signals from pyramidal cells. Finally, the objective approach can be taken (as we have here), which is to make sure for each constraint in the optimization problem to be feasible by limiting the value of β_i (and hence the inflation) with a statistical means.

D. The Effect of Normalization on Bias Removal

As explained in the Linearly Constrained Minimum Variance (LCMV) section, normalization acts as a tool to remove the inherent bias of adaptive beamformers toward deeper locations. In order to investigate this issue, Fig. S4 plots the DLE for the aforementioned beamformers with respect to the depth of source activity (SNR is set to 5 dB). Depth in this figure is defined as the distance between each active node in a source configuration and the nearest electrode (see Fig. S5, which provides some sense about the depth of different brain regions). The plots in Fig. S4 display the localization error over 5 depth intervals. According to this figure, while error is generally expected to increase as activities become deeper (since SNR decreases with depth) the LCMV and RMVB act worse in localizing superficial activities for high levels of noise. Although, the trend for LCVM-ND-DN and RMVB-ND-DN is as expected (higher errors for deeper sources). This observation reflects the mentioned inherent bias of the LCMV and RMVB towards deeper sources and the fact that normalization is quite successful in dealing with this depth-bias issue. Furthermore, it can be observed that once superficial sources are removed from the set of simulated sources, the RMVB results become slightly superior to the LCMV-ND-DN and comparable to the RMVB-ND-DN.

E. The Effect of Correlated Activities

Correlation between distinct sources is known to affect the performance of ESI techniques and particularly beamformers in a negative way. In order to investigate this issue, the third scenario was designed with 100 three-node source configurations, which were highly correlated. Fig. S6 (A) and (B) display the results of this scenario in terms of DLE and output SNR, respectively. It can be seen that correlated activity can degrade the performance mostly in terms of SNR. Although, its effect on DLE is not so severe. Besides, it can be seen that neither normalization and denoising nor the robust modeling of the uncertainty can help to alleviate this condition. Therefore, dealing with correlated activity calls for a separate strategy. It should also be mentioned that the spatially distinct sources are less likely to be maximally correlated [4]. Besides, based on the results of this study, the perfect correlation between the sources that are also spatially coherent (i.e., the dipoles that have the same time-course of activity within the extended sources simulated in the fourth scenario), do not negatively affect the performance in a severe manner. Given the scope of this work, the full investigation of this issue can be the topic of a separate study.

F. Beamformers with Diagonal Loading

In beamformers with diagonal loading, the covariance matrix of the measurements is replaced with a regularized version in which a constant factor (λ) of the unity matrix is added to the measurements covariance matrix. While λ can determine the ultimate quality of reconstruction, its optimal value is unknown. It is proposed in [1] that λ be set to $10\sigma^2$ where σ^2 is the variance of noise. In this study, we have simulated LCMV with diagonal loading (LCMV+DL) using this factor as well as two other values, namely, σ^2 and $100\sigma^2$. The variance of noise in our simulation is calculated by averaging over the diagonal elements of the noise covariance matrix which is determined using baseline. Fig. S7 and Fig. S8, which show the statistical results of LCMV+DL in the second and fourth scenarios, suggest that diagonal loading can improve the reconstruction compared to conventional LCMV. Although, the performance is overall worse than other beamformers introduced in this study. More specifically, it can be observed that RMVB outperforms LCMV+DL based on all metrics and in almost all situations. The only exception is when the noise level is high (SNR=5dB) and the brain activities are focal. In this case, by setting the diagonal loading factor to a high value ($100\sigma^2$), one can improve the performance in the sense of output SNR. Although, RMVB still works better than LCMV+DL according to other metrics and in all other situations. It should also be noted that the mentioned improvement of output SNR is obtained at the cost of losing spatial resolution in the solution of LCMV+DL. Furthermore, RMVB-ND-DN outperforms LCMV+DL in all situations and based on all metrics.

REFERENCES

[1] S. Boyd and L. Vandenberghe, *Convex optimization*. Cambridge university press, 2004.

[2] F. Alizadeh and D. Goldfarb, "Second-order cone programming," *Math. Program.*, vol. 95, no. 1, pp. 3–51, 2003.

[3] D. A. Engemann and A. Gramfort, "Automated model selection in covariance estimation and spatial whitening of MEG and EEG signals," *NeuroImage*, vol. 108, pp. 328–342, 2015.

[4] B. D. Van Veen, W. Van Drongelen, M. Yuchtman, and A. Suzuki, "Localization of brain electrical activity via linearly constrained minimum variance spatial filtering," *IEEE Trans. Biomed. Eng.*, vol. 44, no. 9, pp. 867–880, 1997.

[5] S. A. Vorobyov, A. B. Gershman, and Z.-Q. Luo, "Robust adaptive beamforming using worst-case performance optimization: a solution to the signal mismatch problem," *IEEE Trans. Signal Process.*, vol. 51, no. 2, pp. 313–324, Feb. 2003.

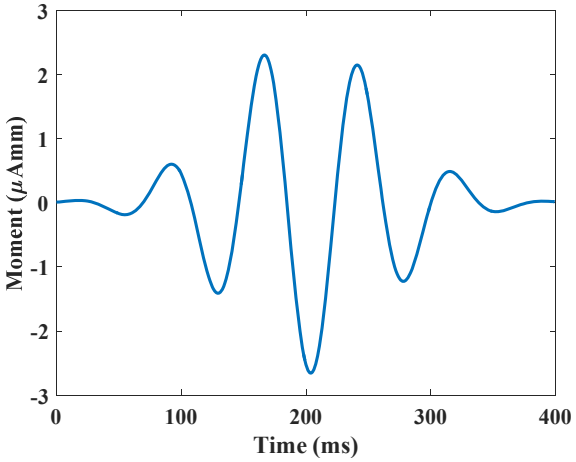

Fig. S1. The time-course assigned to each dipole in the single-node source scenario.

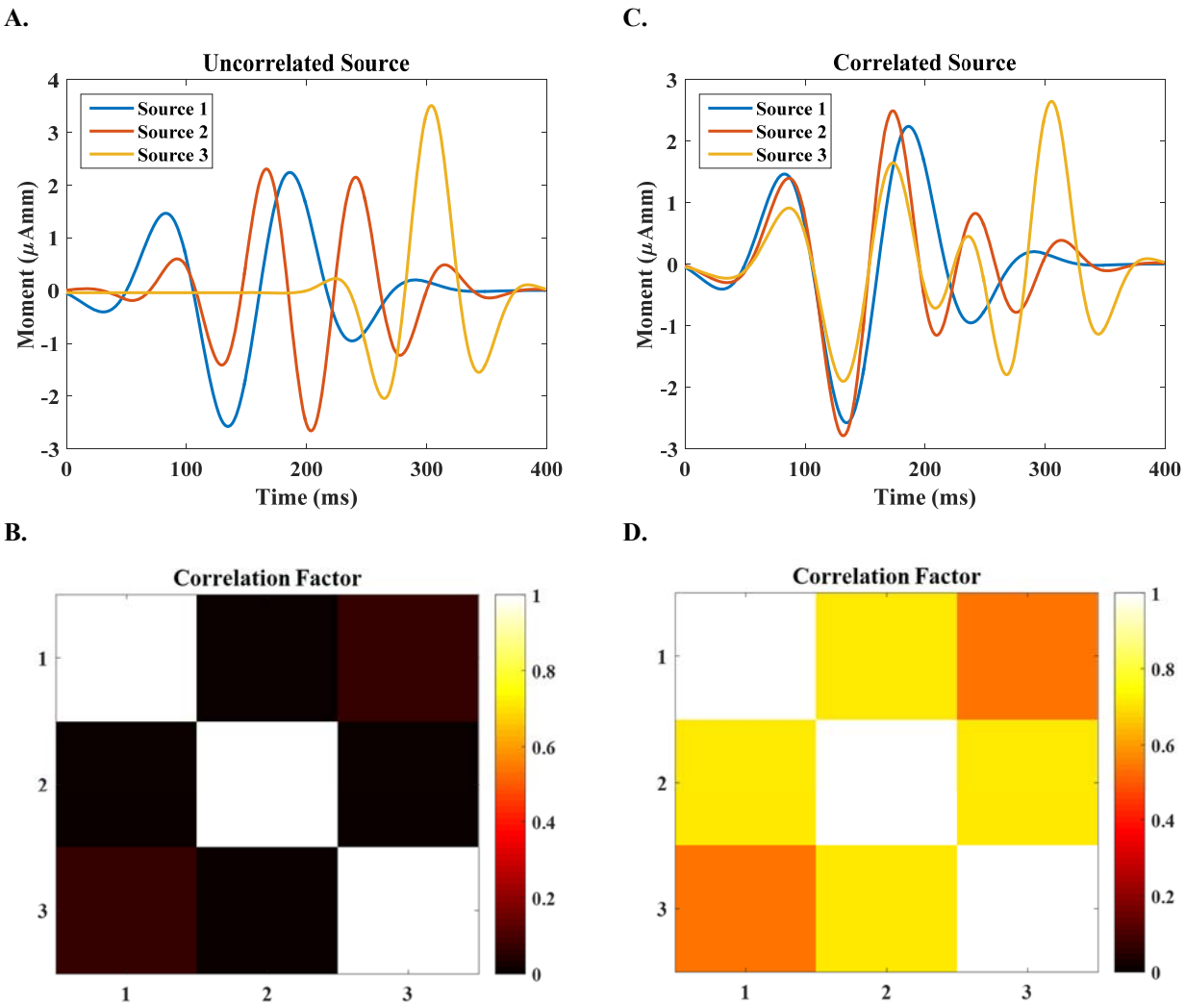

Fig. S2. The time-courses and correlation diagrams in the second and third scenarios. (A) The time-courses assigned to each node in the 3-node uncorrelated source scenario and (B) the corresponding correlation coefficients among the nodes. As it can be seen, the correlation coefficient between different nodes is small in this scenario. (C) The time-courses assigned to each node in the 3-node correlated source scenario and (D) the corresponding correlation coefficients among the nodes. Unlike the second scenario, nodes are highly correlated in this case.

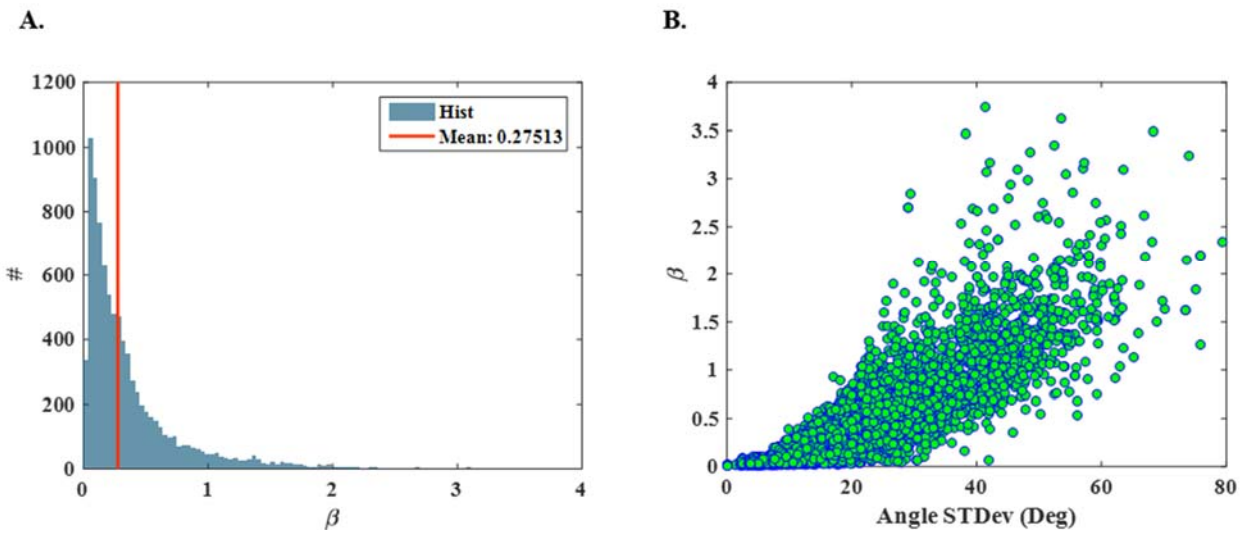

Fig. S3. The histogram of the parameter β and its correlation with angle standard deviation within a region. (A) Plots the histogram of the parameter β and provides information regarding the distribution of the mentioned parameter for all voxels. Red vertical line marks the position of the cut-off value in this distribution. (B) Parameter β of all voxels versus the standard deviation (STDev) of the angle between the center and the neighbors' orientations in each uncertainty region.

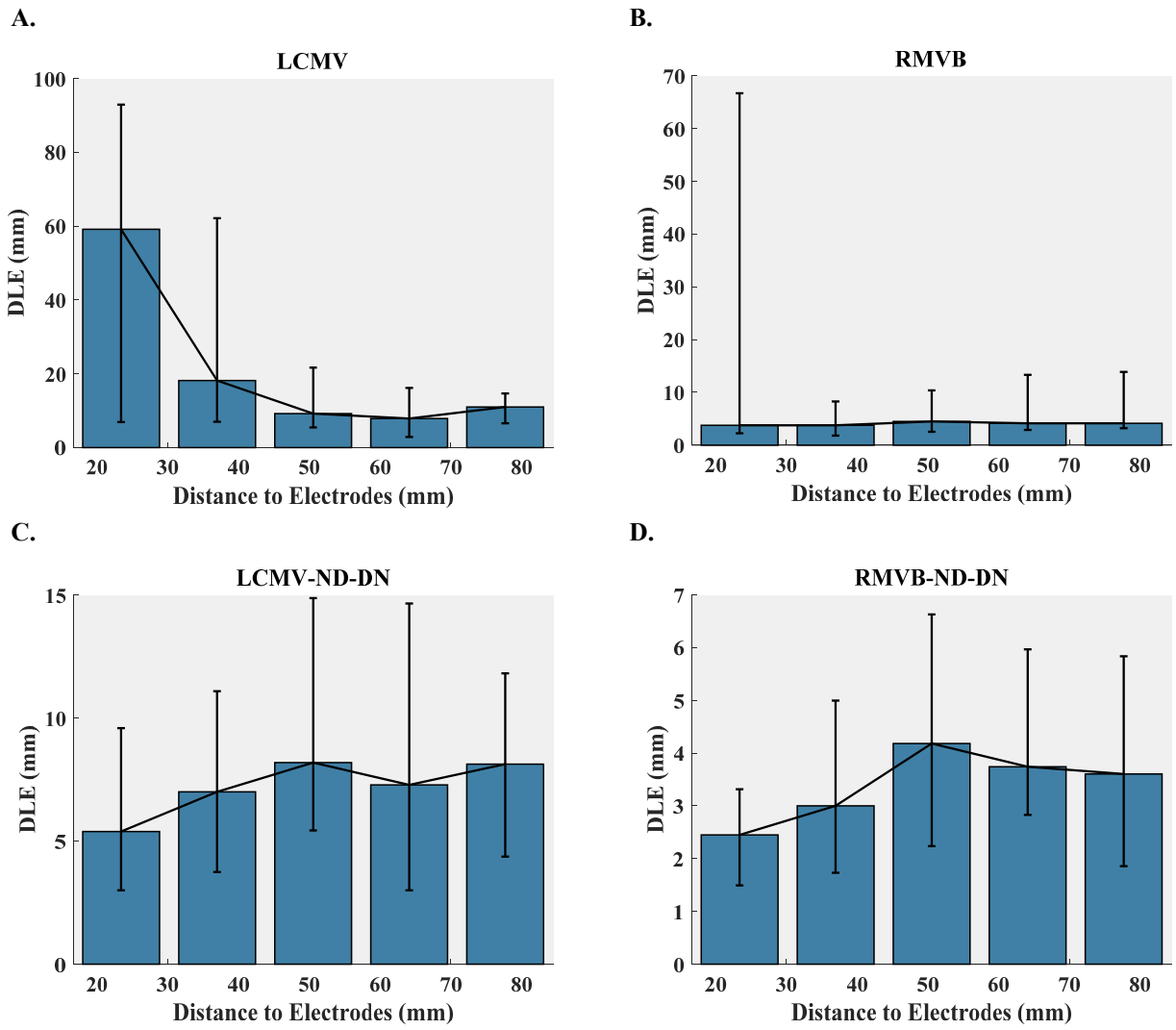

Fig. S4. The DLE results versus depth for the three-node uncorrelated source scenario. The plots display the median DLE along with the error bars over five depth intervals for (A) LCMV, (B) RMVB, (C) LCMV-ND-DN and (D) RMVB-ND-DN. SNR in this figure is set to 5dB and depth is defined as the distance between each active node in a source configuration and the nearest electrode in a standard 128-cahnnel BioSemi cap.

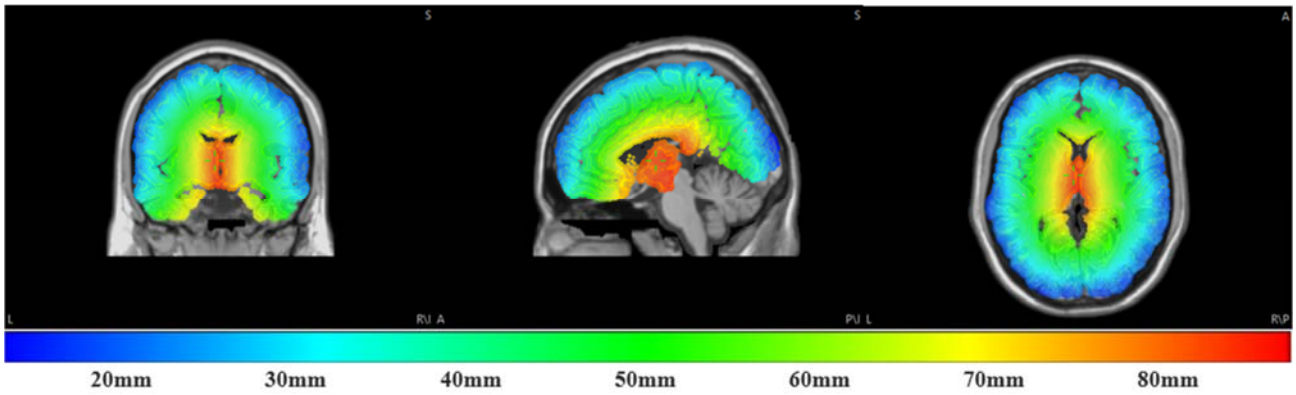

Fig. S5. The color-coded depth of different locations in the brain. Depth in this diagram is defined as the distance to the nearest electrode in a standard 128-cahnnel BioSemi cap.

A. **B.**

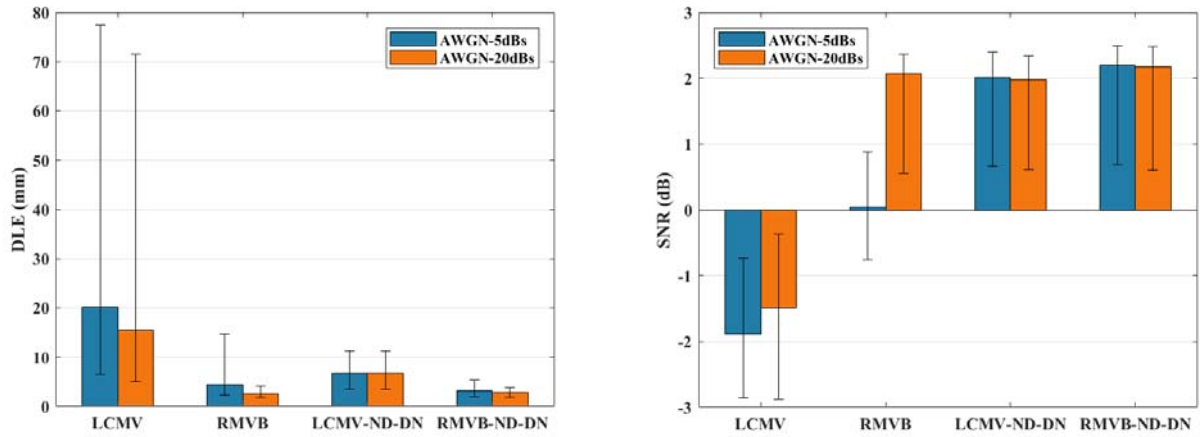

Fig. S6. The Monte Carlo simulation statistics for the three-node correlated source scenario. (A) The median DLE results for SNRs of 5dB and 20dB and for four types of beamformers namely, LCMV, RMVB, LCMV-ND-DN and RMVB-ND-DN. The error bars mark the first and third quartiles (of DLE distribution). (B) The median output SNR results along with the first and third quartile error bars for the same configuration.

A. **B.**

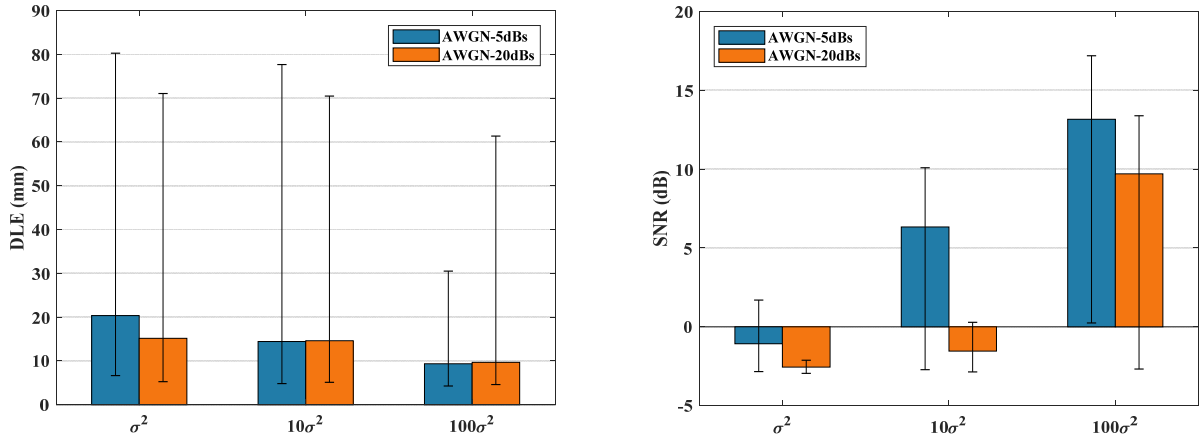

Fig. S7. The Monte Carlo simulation statistics for the three-node uncorrelated source scenario. (A) The median DLE results for SNRs of 5dB and 20dB and for diagonal loading beamformer with three factors namely, σ^2 $10\sigma^2$ and $100\sigma^2$. The error bars mark the first and third quartiles (of DLE distribution). (B) The median output SNR results along with the first and third quartile error bars for the same configuration.

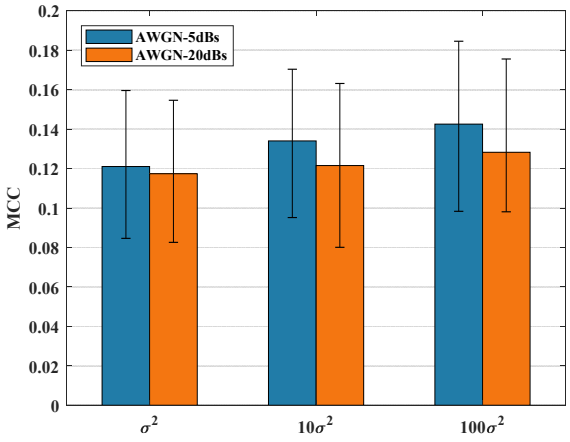

Fig. S8. The Monte Carlo simulation statistics for the extended source scenario. The median MCC results along with the first and third quartile error bars for diagonal loading beamformer with three factors namely, σ^2, $10\sigma^2$ and $100\sigma^2$ and for SNR of 20 dB.